Available online at www.sciencedirect.com
ScienceDirect
International Journal of Heat and Fluid Flow 28 (2007) 720–734
International Journal of HEAT AND FLUID FLOW
www.elsevier.com/locate/ijhff

Numerical analysis of heat transfer on a rotating disk surface under confined liquid jet impingement

Jorge C. Lallave, Muhammad M. Rahman *, Ashok Kumar

Department of Mechanical Engineering, University of South Florida, 4202 East Fowler Avenue, ENB 118, Tampa, FL 33620, United States

Received 7 November 2005; received in revised form 24 September 2006; accepted 24 September 2006
Available online 14 December 2006

Abstract

The objective of this study is to characterize the conjugate heat transfer for a confined liquid jet impinging on a rotating and uniformly heated solid disk of finite thickness and radius. The model covers the entire fluid region (impinging jet and flow spreading out over the rotating surface) and the solid disk as a conjugate problem. Calculations were done for a number of disk materials and working fluids covering a range of Reynolds number (500–1500), under a broad rotational rate range of 0–750 rpm or Ekman number (4.42×10^{-5} to ∞), nozzle to target spacing ($\beta = 0.25$–5.0), disk thicknesses to nozzle diameter ratio ($b/d_n = 0.167$–1.67), Biot number (3.73×10^{-3}–0.118), Prandtl number (1.29–124.44), and solid to fluid thermal conductivity ratio (36.91–2222). It was found that plate materials with higher thermal conductivity maintained a more uniform temperature distribution at the solid–fluid interface. A higher Reynolds number increased the local heat transfer coefficient reducing the wall to fluid temperature difference over the entire interface. The rotational rate also increased local heat transfer coefficient under most conditions. The simulation results compared reasonably well with previous experimental studies.

Keywords: Jet impingement; Rotating disk; Conjugate heat transfer

1. Introduction

Heat transfer capabilities of jets impingining on a rotating body is of importance in the thermal analysis of various types of machineries and in a wide variety of applications in the area of thermal heating and cooling. Processes like turbine blade cooling, annealing of metal, tempering of glass, chemical vapor deposition, avionics cooling, electronics packaging, etc. can use this technique. The principal virtues of jet impingement are a large heat transfer rate and the relative ease with which both the heat transfer rate and distribution can be controlled. Secondly, the rotation is an effective way to generate secondary flow and therefore enhance heat transfer. The interaction of rotation and impingement creates a very complex and powerful flow capable of improving heat transfer processes considerably.

Heat transfer from a stationary surface by liquid jet impingement has been reported by Saad et al. (1977). They investigated the effects of Reynolds number, distance between nozzle and impingement surface, diameters of impingement and confinement surfaces, and shape of the velocity profile at the nozzle exit. Nakoryakov et al. (1978) studied theoretically and experimentally the hydrodynamics and mass transfer of a radial submerged liquid jet impinging onto a horizontal plane. Their study measured the wall shear stress, local and mean mass transfer coefficients within the entire flow. Jiji and Dagan (1987) carried out experimental studies for single jet and arrays of jets using water and FC-77 coolant for various heat source configurations. Polat et al. (1989) presented a comprehensive review of studies on laminar and turbulent jets impinging on flat surfaces under a limited range of relevant parameters. The authors concluded that the two-equation and algebraic stress models, which allow the integration of variables up to the wall, provides the best hope for

* Corresponding author. Tel.: +1 813 974 5625; fax: +1 813 974 3539.
E-mail address: rahman@eng.usf.edu (M.M. Rahman).

0142-727X/$ - see front matter © 2006 Elsevier Inc. All rights reserved.
doi:10.1016/j.ijheatfluidflow.2006.09.005

Nomenclature

Bi	Biot number, $(h_{av} \cdot b)/k_S$
C_p	specific heat (J/kg K)
d_n	diameter of the nozzle (m)
g	acceleration due to gravity (m/s^2)
Ek	Ekman number, $\nu_f/(4 \cdot \Omega \cdot r_d^2)$
h	heat transfer coefficient (W/m^2 K), $q_{int}/(T_{int} - T_J)$
H_n	height of the nozzle from the plate (m)
k	thermal conductivity (W/m K)
nr	number of elements in radial direction
nZ	number of elements in axial direction
Nu	Nusselt number, $(h \cdot d_n)/k_f$
Nu_{av}	average Nusselt number for the entire surface, $(h_{av} \cdot d_n)/k_f$
p	pressure (Pa)
Pr	Prandtl number, ν_f/α_f
q	heat flux (W/m^2)
r	radial coordinate (m)
r_d	disk radius (m)
Re	Reynolds number, $(V_J \cdot d_n)/\nu_f$
T	temperature (K)
V_J	jet velocity (m/s)
$V_{r,Z,\theta}$	velocity component in the r, z, θ-direction (m/s)
z	axial coordinate (m)

Greek symbols

α	thermal diffusivity (m^2/s)
β	dimensionless nozzle to target spacing, H_n/d_n
ε	thermal conductivity ratio, k_S/k_f
μ	dynamic viscocity (kg/m s)
ν	kinematic viscosity (m^2/s)
θ	angular coordinate (rad)
Θ	dimensionless temperature, $2 \cdot k_f \cdot (T_{int} - T_J)/(q \cdot d_n)$
ρ	density (kg/m^3)
Ω	angular velocity (rad/s)

Subscripts

atm	ambient
av	average
f	fluid
int	solid–fluid interface
J	jet or inlet
max	maximum
n	nozzle
S	solid

engineering calculations for turbulent impinging jets in near future.

Polat et al. (1991a) measured local and average heat transfer coefficients for a confined turbulent slot jet impinging on a permeable surface with thorough flow. Measurements were carried out for a wide range of jet Reynolds number and thorough flow velocity. Polat et al. (1991b) measured local and average heat transfer coefficients for a confined turbulent slot jet impinging on a moving surface considering thorough flow. Chang et al. (1993) examined the local heat transfer distribution of a submerged liquid jet under confinement. Hung and Lin (1994) proposed an axisymmetric sub-channel model for evaluating local surface heat flux for confined and unconfined cases. Their models revealed that no significant deviation occurs for stagnation Nusselt numbers at nozzle to target spacing ($H_n/d_n > 2$) while significant deviation exist for $H_n/d_n < 2$. Garimella and Rice (1995) and Fitzgerald and Garimella (1997) presented experimental results for the local heat transfer coefficient as functions of nozzle diameter for submerged liquid and fully turbulent jets using FC-77 as the working fluid.

Webb and Ma (1995) presented a comprehensive review of studies on jet impingement heat transfer. They concluded that heat transfer in submerged jets is more sensitive to nozzle to target spacing than in free jets, especially when the heat transfer surface is beyond the potential core of the jet. Garimella and Nenaydykh (1996) conducted experiments to determine the effects of the nozzle geometry on the local heat transfer coefficient from a small heat source to a normally impinging, axisymmetric, submerged and confined liquid jet of FC-77 at different nozzle to target spacings and Reynolds numbers.

Ma et al. (1997) investigated the radial distribution of the recovery factor for a confined impinging jet of high Prandtl number liquid. They found that the recovery factor is strongly dependent on the Prandtl number, nozzle to target spacing, and the velocity profile at the nozzle exit, but basically independent of the Reynolds number. Li and Garimella (2001) studied the effects of fluid thermophysical properties on heat transfer from a confined and submerged impinging jet. Local heat transfer coefficients were obtained experimentally from a discrete heat source. A generalized correlation was reported for the Prandtl number range of 0.7–25.2. Roy et al. (2002) reported surface temperature measurements for rectangular jet impingement heat transfer on a vehicle windshield using liquid crystals. Chan et al. (2002) reported experimental results on heat transfer characteristics of a heated slot jet impinging on a semi-circular convex surface. Ichimiya and Yamada (2003) presented the heat transfer and fluid flow characteristics of a single circular laminar impinging jet including buoyancy force in a comparatively narrow space with a confining wall. They identified the presence of forced, mixed, and natural convection modes of heat transfer as the flow moved downstream in the radial direction.

Shi et al. (2003) presented a numerical study to examine the effects of thermophysical properties for semi-confined laminar slot jet. The fluid Prandtl number ranged from 0.7 to 71. Local, stagnation, and average values of the impingement Nusselt number were reported. Tong (2003) presented a numerical investigation of convective heat transfer of a circular liquid jet impinging onto a substrate. The effects of several key parameters on the hydrodynamics and heat transfer of an impinging liquid jet were examined. Silverman and Nagler (2004) reported experimental data on the application of jet impingement for the cooling of accelerator targets using water as the coolant. El-Gabry and Kaminski (2005) presented experimental measurements of local heat transfer distribution on smooth and roughened surfaces under an array of angled impinging jets. Liquid crystal video thermography was used to capture surface temperature data at five different jet Reynolds number ranging from 15,000 to 35,000.

The jet impingement on a rotating disk adds more complexity to the flow field. Carper and Deffenbaugh (1978) conducted experiments to determine the average heat transfer coefficients for the rotating solid-fluid interface, with uniform temperature, cooled by a single liquid jet of oil impinging normal to the rotating disk. Their tests were conducted over a range of flow rates and disk rotational speeds with various combinations of jet nozzle diameter and disk diameter. A non-dimensional correlation was given in terms of jet and rotational Reynolds numbers. Mochizuki and Inoue (1990) conducted experiments to determine the fluid flow and heat transfer characteristics in a passage formed by two parallel rotating disks. Local heat transfer coefficient distribution along the disk radius was measured using an electrically conductive plastic film and flow patterns were visualized by using paraffin mist and a laser-light sheet. Thomas et al. (1991) measured the film thickness across a stationary and rotating horizontal disk using the capacitance technique, where the liquid was delivered to the disk by a controlled impinging jet. The aim was to provide an understanding of the fundamental hydrodynamic processes that occur in the flow. In a later study, Faghri et al. (1993) presented heat transfer measurements and numerical simulation of the free surface problem for different volumetric flow rates and inlet temperatures. The numerical predictions agreed with experimental measurements. Metzger et al. (1991) employed liquid crystal for mapping local heat transfer distributions on a rotating disk with jet impingement.

Saniei et al. (1998) investigated the heat transfer coefficients from a rotating disk with jet impingement at its geometric center. The jet was placed perpendicular to the disk surface at four different distances from the center of the disk. Saniei and Yan (2000) presented local heat transfer measurements for a rotating disk cooled with an impinging air jet. Several important factors such as rotational Reynolds number, jet Reynolds number, jet-to-disk spacing, and the location of the jet center relative to the disk center were examined. Hung and Shieh (2001) reported experimental measurements of heat transfer characteristics of jet impingement onto a horizontally rotating ceramic-based multichip disk. The chip temperature distributions along with local and average Nusselt numbers were presented. Kang and Yoo (2002) carried out an experimental study using hotwire anemometry to investigate the turbulence characteristics of the three-dimensional boundary layer on a rotating disk with jet impingement at its center. Shevchuk et al. (2003) presented an approximate analytical solution using integral method for jet impingement heat transfer over a rotating disk. Iacovides et al. (2005) reported an experimental study of impingement cooling in a rotating passage of semi-cylindrical cross-section. Cooling fluid was injected from a row of five jet holes along the centerline of the flat surface of the passage and impinged the concave surface.

From the above literature review it can be noticed that even though jet impingement heat transfer from a stationary surface has been quite thoroughly investigated, mainly experimental results are available for jet impingement over a rotating disk, and these studies are primarily for free jet without any confinement. The detailed information about conjugate heat transfer (covering the solid disk and cooling fluid) from a rotating disk cooled by a confined liquid jet is currently not available in open literature. The objective of the present research is to study conjugate heat transfer effect with a steady flow over a rotating solid wafer confined by a stationary disk to investigate how the heat transfer is affected by the rotation of the disk. Computations using water, ammonia, flouroinert, and lubricating oil as working fluids were carried out for a set of different flow configurations, including four different disk materials for various flow and spinning rates. The results offer a better understanding of the fluid mechanics and heat transfer behavior of jet impingement on a spinning disk. Even though no new numerical technique has been developed, results obtained in the present investigation are entirely new. The numerical results showing the quantitative effects of different parameters as well as the correlation for average Nusselt number will be practical guides for design engineers.

2. Analysis and computation

A three-dimensional representation of the confined axial jet impinging perpendicularly on a uniformly heated spinning solid wafer corresponds to two parallel disks as shown in Fig. 1. The liquid jet is discharged through an orifice at the center of the top disk. The remainder of the top disk acts as an insulated stationary confinement plate. The bottom disk (wafer) is subjected to a uniform angular velocity. Heat sources are located at the bottom of the wafer producing a constant heat flux at that surface. Heat is conducted through the wafer and convected out to the fluid adjacent to the top surface of the wafer as shown in Fig. 1. The present study considered an incompressible, Newtonian, and axisymmetric flow under a steady state

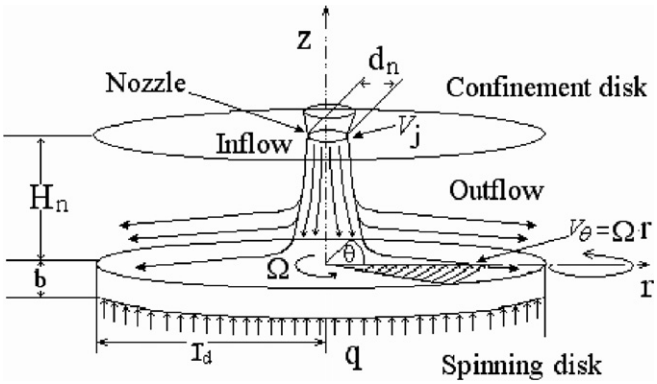

Fig. 1. Three-dimensional schematic of axisymmetric confined liquid jet impingement on a uniformly heated spinning disk.

condition. The variation of fluid properties with local temperature was taken into account. Due to rotational symmetry of the problem the $\partial/\partial\theta$ terms could be omitted. The equations describing the conservation of mass, momentum (r-, θ- and z-directions, respectively), and energy can be written as (Burmeister, 1993):

$$\frac{1}{r}\frac{\partial}{\partial r}(\rho_f r V_r) + \frac{\partial}{\partial z}(\rho_f V_Z) = 0 \tag{1}$$

$$\rho_f\left(V_r\frac{\partial V_r}{\partial r} + V_Z\frac{\partial V_r}{\partial z} - \frac{V_\theta^2}{r}\right) = -\frac{\partial p}{\partial r} + \frac{1}{r}\frac{\partial}{\partial r}\left[\frac{2}{3}\cdot\mu_f r\left(2\frac{\partial V_r}{\partial r} - \frac{V_r}{r} - \frac{\partial V_Z}{\partial z}\right)\right] + \frac{\partial}{\partial z}\left[\mu_f\left(\frac{\partial V_r}{\partial z} + \frac{\partial V_Z}{\partial r}\right)\right] + \frac{2}{3}\cdot\frac{\mu_f}{r}\left(\frac{\partial V_r}{\partial r} + \frac{\partial V_Z}{\partial z} - \frac{2\cdot V_r}{r}\right) \tag{2}$$

$$\rho_f\left(V_r\frac{\partial V_\theta}{\partial r} + V_Z\frac{\partial V_\theta}{\partial z} + \frac{V_r V_\theta}{r}\right) = \frac{1}{r^2}\frac{\partial}{\partial r}\left[r^2\mu_f\left[r\frac{\partial}{\partial r}\left(\frac{V_\theta}{r}\right)\right]\right] + \frac{\partial}{\partial z}\left[\mu_f\left(\frac{\partial V_\theta}{\partial z}\right)\right] \tag{3}$$

$$\rho_f\left(V_r\frac{\partial V_Z}{\partial r} + V_Z\frac{\partial V_Z}{\partial z}\right) = -\rho_f g - \frac{\partial p}{\partial z} + \frac{1}{r}\frac{\partial}{\partial r}\left[r\mu_f\left(\frac{\partial V_r}{\partial z} + \frac{\partial V_Z}{\partial r}\right)\right] + \frac{\partial}{\partial z}\left[\frac{2}{3}\mu_f\left(2\frac{\partial V_Z}{\partial z} - \frac{V_r}{r} - \frac{\partial V_r}{\partial r}\right)\right] \tag{4}$$

$$\rho_f\left(V_r\frac{\partial(C_{p_f}T_f)}{\partial r} + V_Z\frac{\partial(C_{p_f}T_f)}{\partial z}\right) = \left[\frac{1}{r}\frac{\partial}{\partial r}\left(k_f r\frac{\partial T_f}{\partial r}\right) + \frac{\partial}{\partial z}\left(k_f\frac{\partial T_f}{\partial z}\right)\right] + 2\cdot\mu_f\left[\left(\frac{\partial V_r}{\partial r}\right)^2 + \left(\frac{V_r}{r}\right)^2 + \left(\frac{\partial V_Z}{\partial z}\right)^2 + \frac{1}{2}\left(\frac{\partial V_\theta}{\partial r} - \frac{V_\theta}{r}\right)^2 + \frac{1}{2}\left(\frac{\partial V_\theta}{\partial z}\right)^2 + \frac{1}{2}\left(\frac{\partial V_r}{\partial z} + \frac{\partial V_Z}{\partial r}\right)^2 - \frac{1}{3}\left(\frac{\partial V_r}{\partial r} + \frac{V_r}{r} + \frac{\partial V_Z}{\partial z}\right)^2\right] \tag{5}$$

The variation of thermal conductivity of solids with temperature was not significant. Therefore, the conservation of energy inside the solid can be characterized by the following equation:

$$\frac{\partial^2 T_S}{\partial r^2} + \frac{1}{r}\left(\frac{\partial T_S}{\partial r}\right) + \frac{\partial^2 T_S}{\partial z^2} = 0 \tag{6}$$

The following boundary conditions were used to fulfill the physical problem formulation:

$$\text{At } r = 0,\ -b \leqslant z \leqslant 0 : \frac{\partial T_S}{\partial r} = 0 \tag{7}$$

$$\text{At } r = 0,\ 0 \leqslant z \leqslant H_n : V_\theta = V_r = 0,\ \frac{\partial V_Z}{\partial r} = 0,\ \frac{\partial T_f}{\partial r} = 0 \tag{8}$$

$$\text{At } r = r_d,\ -b \leqslant z \leqslant 0 : \frac{\partial T_S}{\partial r} = 0 \tag{9}$$

$$\text{At } r = r_d,\ 0 \leqslant z \leqslant H_n : p = p_{atm} \tag{10}$$

$$\text{At } z = -b,\ 0 \leqslant r \leqslant r_d : -k_S\frac{\partial T_S}{\partial z} = q \tag{11}$$

$$\text{At } z = 0,\ 0 \leqslant r \leqslant r_d : V_\theta = \Omega\cdot r,\ V_r = V_Z = 0,\ T_f = T_S,\ k_S\frac{\partial T_S}{\partial z} = k_f\frac{\partial T_f}{\partial z} \tag{12}$$

$$\text{At } z = H_n,\ 0 \leqslant r \leqslant \frac{d_n}{2} : V_Z = -V_J,\ V_r = V_\theta = 0,\ T_f = T_J \tag{13}$$

$$\text{At } z = H_n,\ \frac{d_n}{2} \leqslant r \leqslant r_d : V_r = V_Z = V_\theta = 0,\ \frac{\partial T_f}{\partial z} = 0 \tag{14}$$

The local and average heat transfer coefficients can be defined as

$$h = \frac{q}{(T_{int} - T_J)} \tag{15}$$

$$h_{av} = \frac{2}{r_d^2\cdot(\overline{T}_{int} - T_J)}\int_0^{r_d} h_r(T_{int} - T_J)\mathrm{d}r \tag{16}$$

where $\overline{T}_{int}$ is the average temperature at the solid–liquid interface. The local and average Nusselt numbers are calculated according to the following expressions:

$$Nu = \frac{h\cdot d_n}{k_f} \tag{17}$$

$$Nu_{av} = \frac{h_{av}\cdot d_n}{k_f} \tag{18}$$

Essentially a rotating laminar flow under jet impingement is controlled by three major physical parameters: the Reynolds number, $Re_J = V_J d_n/\nu_f$, the dimensionless nozzle to target spacing ratio, $\beta = H_n/d_n$, and the Ekman number, $Ek = \nu_f/4\cdot\Omega\cdot r_d^2$. The top disk remains stationary while the bottom disk rotates at a uniform angular velocity. The values of Reynolds number was limited to a maximum of 1500 to stay within the laminar region. Two different nozzle diameters were used with values of 0.6 and 1.2 mm. The heat flux (q) was also kept constant at 250 kW/m^2, although the disk radius was set for two different values of 7.6 and 6.0 mm. The incoming fluid temperature (T_J) was 303 K for water, FC-77 and Ammonia (at a pressure of 20 bars), and 373 K for MIL-7808. The thickness of the disk was varied over the following values: 0.3, 0.6, 0.9, 1.20, 1.5 and 2.0 mm. The jet impingement height

or the distance between the nozzle and disk was set at the following values: 1.50×10^{-4}, 3.0×10^{-4}, 6.0×10^{-4}, 1.20×10^{-3}, 1.80×10^{-3}, 2.40×10^{-3}, and 3.0×10^{-3} m. The spinning rate (Ω) was varied from 0 to 78.54 rad/s or 0 to 750 rpm. The flow rate was varied from 1.89×10^{-7} to 7.55×10^{-7} m^3/s. The range for Reynolds number and Ekman number were: $Re = 500$ to 1500 and $Ek = 4.42\times10^{-5}$ to ∞. The possibility of getting into turbulent flow due to disk rotation was checked. Using the laminar-turbulent transition criterion used by Popiel and Boguslawski (1986) and Vanyo (1993) all runs used in the paper checked out to be laminar. The simulation was carried out for a number of disk materials, namely Constantan, copper, aluminum, silicon, and silver.

The properties of solid materials were obtained from Özisik (1993). Fluid properties for H_2O, NH_3, MIL-7808, and FC-77 were obtained from Bejan (1995), Brady vendor, and 3M Specialty Fluids, respectively. The properties of the above fluids can be written according to the following equations. For water between $300\text{ K} < T < 411\text{ K}$; $C_{p_f} = 9.5\times10^{-3}\cdot T^2 - 5.9299\cdot T + 5098.1$; $k_f = -7.0\times10^{-6}\cdot T^2 + 5.8\times10^{-3}\cdot T - 0.4765$; $\rho_f = -2.7\times10^{-3}\cdot T^2 + 1.3104\cdot T + 848.07$; and $\ln(\mu_f) = -3.27017 - 0.0131\cdot T$. For ammonia between $273.15\text{ K} < T < 370\text{ K}$; $C_{p_f} = 0.083\cdot T^2 - 40.489\cdot T + 9468$; $k_f = 1.159 - 2.30\times10^{-3}\cdot T$; $\rho_f = 579.81 + 1.6858\cdot T - 0.0054\cdot T^2$; and $\ln(\mu_f) = -5.33914 - 0.0115\cdot T$. For MIL-7808 between $303\text{ K} < T < 470\text{ K}$; $C_{p_f} = 903.8 + 3.332\cdot T$; $k_f = 0.18 - 1\times10^{-4}\cdot T$; $\rho_f = 1181 - 0.708\cdot T$; and $\ln(\mu_f) = 3.2436 - 0.0229\cdot T$. For FC-77 between $273\text{ K} < T < 380\text{ K}$; $C_{p_f} = 589.2 + 1.554\cdot T$; $k_f = 0.0869 - 8\times10^{-5}\cdot T$; $\rho_f = 2507.2 - 2.45\cdot T$; and $\ln(\mu_f) = -2.38271 - 0.0145\cdot T$. In these correlations, the absolute temperature T was used in K.

The governing equations (1)–(6) along with the boundary conditions (7)–(14) were solved using the Galerkin finite element method (Fletcher, 1984). Four node quadrilateral elements were used. In each element, the velocity, pressure, and temperature fields were approximated which led to a set of equations that defined the continuum. A denser grid distribution was used near the solid–fluid interface to adequately capture large variations in that region. The solution of the resulting non-linear differential equations was carried out using the Newton–Raphson method. Due to non-linear nature of the governing transport equations, an iterative procedure was used to arrive at the solution for the velocity and temperature fields. The solution was considered converged when the field values did not change from one iteration to the next and the sum of the residuals for each variable was less than 10^{-6}.

3. Results and discussion

A typical velocity vector distribution is shown in Fig. 2. It can be seen that the velocity remains almost uniform at the potential core region of the jet. The velocity decreases and the fluid jet diameter increases as the fluid gets closer to the plate during the impingement process. Thereafter, the fluid strikes the solid surface at which point there is a rapid deceleration while the flow changes direction parallel to the solid disk. After this, there is a brief acceleration starting the development of boundary layer. It can be noticed that the boundary layer thickness increases along the radius. The fluid between the boundary layer zone and confined top plate remains quasi-stagnant with a flow velocity one-tenth or less than the inlet velocity. The solid–fluid dimensionless interface temperatures for different number of grids are plotted in Fig. 3. Several grids were used to determine the number of elements needed for accurate numerical solution. It was observed that the numerical solution becomes grid independent when the grids reach a number of divisions equals to 64×79 in the axial (z) and radial (r) directions, respectively. Numerical results for a 64×79 grid gave almost identical results compared to a 100×85 grid for an impingement heights (H_n) equal to 0.32 cm. Therefore, the chosen grid was 64×79 that car-

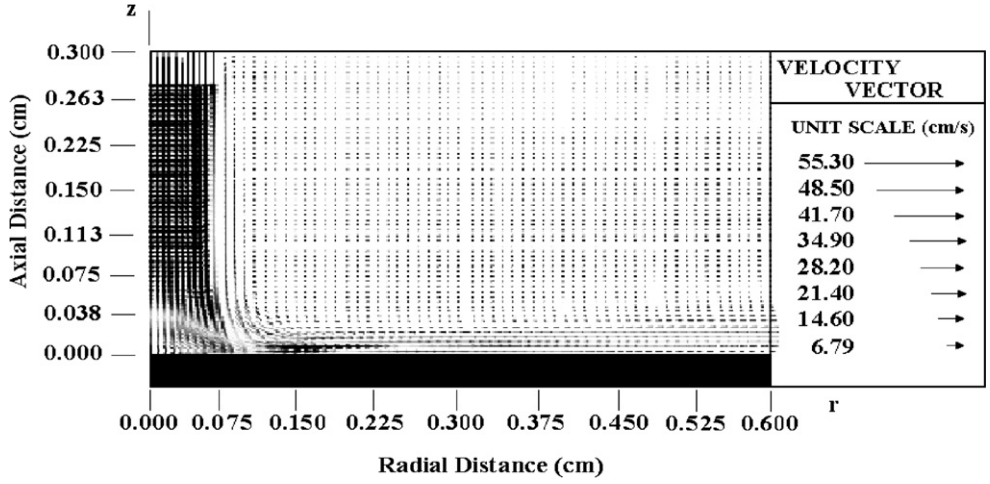

Fig. 2. Velocity vector distribution for a confined jet impingement on a silicon wafer with water as the cooling fluid ($Re = 1000$, $Ek = 9.46\times10^{-5}$, $\beta = 2.67$, $b/d_n = 0.25$).

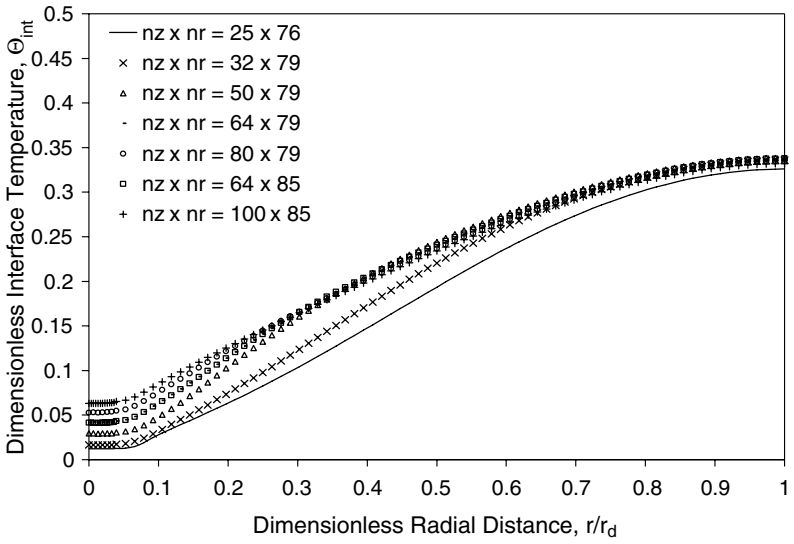

Fig. 3. Dimensionless interface temperature distributions for different number of elements in r- and z-directions ($Re = 1500$, $b = 0$, $d_n = 0.6$ mm, $Ek = 2.65 \times 10^{-4}$, $\beta = 5.333$).

ried an average error margin of 0.35% compared to 100×85 grids.

Fig. 4 shows the variation of the solid–fluid dimensionless interface temperature for different Reynolds number under a low rotational rate ($Ek = 2.65 \times 10^{-4}$). The plots in Fig. 4 reveal that dimensionless interface temperature decreases with jet velocity (or Reynolds number). At any Reynolds number, the interface temperature has the lowest value at the stagnation point (underneath the center of the axial opening) and increases radially along the radius reaching the highest value at the end of the disk. This is due to the development of thermal boundary layer as the fluid moves downstream from the center of the disk. The thickness of the thermal boundary layer increases with radius and causes the interface temperature to increase. It may be noted, however, that due to spinning streamlines are not aligned along the disk radius, rather the fluid moves at an angle based on the rate of rotation. Fig. 5 presents the local Nusselt number distributions along the solid–fluid interface for different Reynolds numbers for the same rotational rate ($Ek = 2.65 \times 10^{-4}$). All local Nusselt number distributions are half-bell shaped with a peak at the stagnation point. Figs. 4 and 5 confirm to us how an increasing Reynolds number contributes to a more effective cooling.

Fig. 6 plots the average Nusselt number as a function of Reynolds number for low, intermediate, and high Ekman numbers. It may be noted that average Nusselt number increases with Reynolds number. As the flow rate

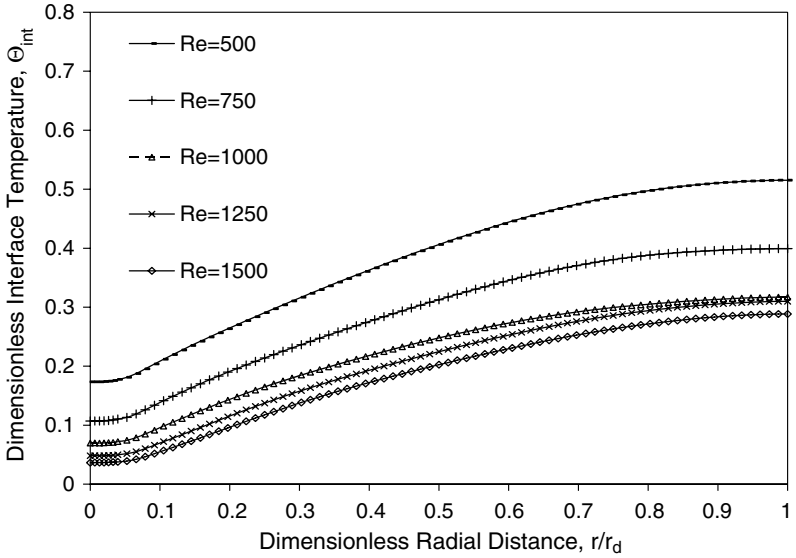

Fig. 4. Dimensionless interface temperature distributions for a silicon wafer with water as the cooling fluid for different Reynolds numbers ($Ek = 2.65 \times 10^{-4}$, $\beta = 5.333$, $b/d_n = 0.5$).

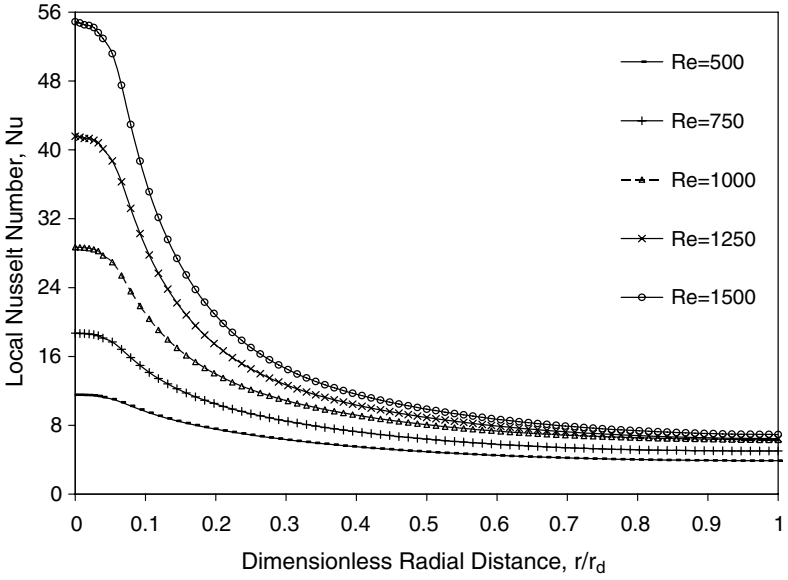

Fig. 5. Local Nusselt number distributions for a silicon wafer with water as the cooling fluid for different Reynolds numbers ($Ek = 2.65 \times 10^{-4}$, $\beta = 5.333$, $b/d_n = 0.5$).

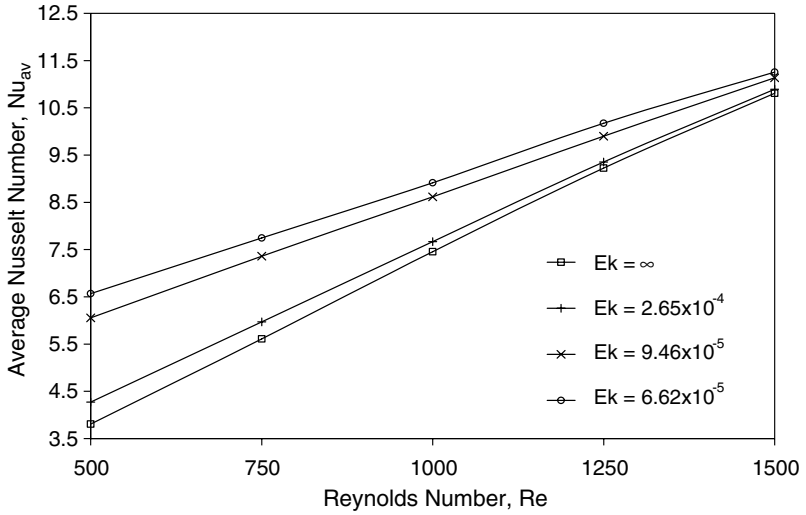

Fig. 6. Average Nusselt number variations with Reynolds number at different Ekman numbers for a silicon wafer with water as the cooling fluid ($\beta = 5.333$, $b/d_n = 0.5$).

(or Reynolds number) increases, the magnitude of fluid velocity near the solid–fluid interface that controls the convective heat transfer rate increases. Furthermore, at a particular Reynolds number, the Nusselt number decreases with Ekman number (or gradually increases with the increment of disk spinning rate). This behavior confirms the positive influence of the rotational rate on the average Nusselt number. It may be noticed that the average Nusselt number plots gets closer to each other as the Reynolds number increases indicating that curves will intersect at higher Reynolds numbers. These intersections indicate the presence of a liquid jet momentum dominated region at higher Reynolds numbers. From the numerical results it was observed that the heat transfer is dominated by impingement when $Re \cdot Ek > 0.1125$ and dominated by disk rotation when $Re \cdot Ek < 0.075$. In between there limits, both of these effects play an important role in determining the variations of average Nusselt number. This type of behavior is consistent with the experimental results of Brodersen et al. (1996a,b) where the ratio of jet and rotational Reynolds numbers was used to characterize the flow regime.

The rotational rate effects on the local Nusselt number and solid–fluid dimensionless interface temperature are illustrated in Figs. 7 and 8. All curves in Fig. 7 portray a half-bell shaped profile with crest at the stagnation region. This trend matches with previous studies by Webb and Ma (1995) and Chang et al. (1993). It may be noted that rotational effect increases local Nusselt number and generates

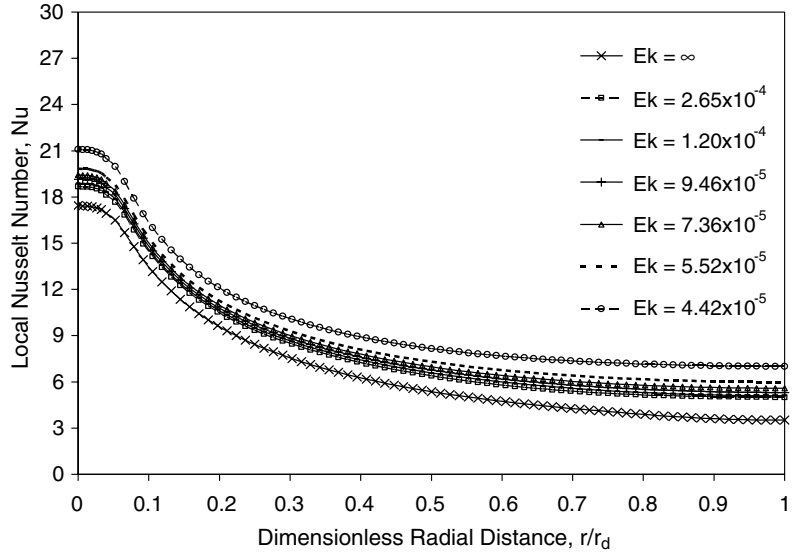

Fig. 7. Local Nusselt number distributions for a silicon wafer with water as the cooling fluid at different Ekman numbers ($Re = 750$, $\beta = 5.333$, $b/d_n = 0.5$).

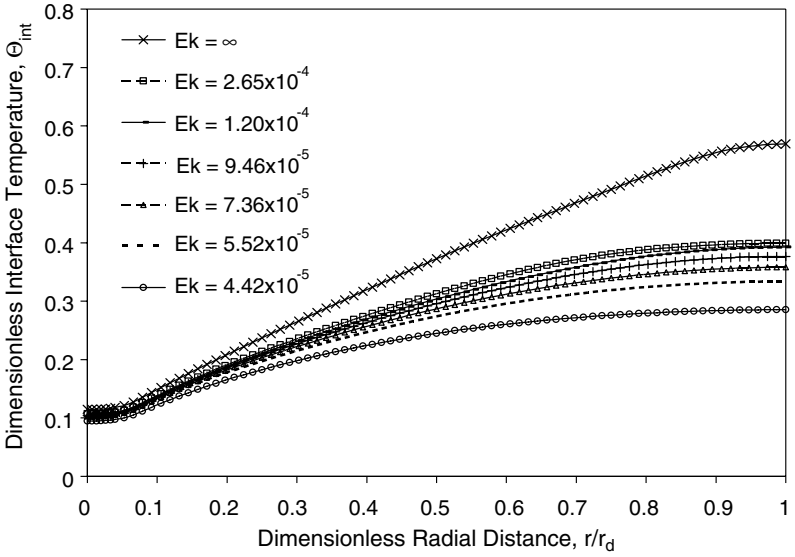

Fig. 8. Dimensionless interface temperature distributions for a silicon wafer with water as the cooling fluid at different Ekman numbers ($Re = 750$, $\beta = 5.333$, $b/d_n = 0.5$).

lower temperature over the entire solid–fluid interface with somewhat less intensity in comparison with the Reynolds number effect. As the Ekman number decreases from ∞ to 4.42×10^{-5} the local Nusselt number increases by an average 25.7% under a low Reynolds number ($Re = 750$). Fig. 8 shows that dimensionless interface temperature decreases with the increment of the rotational rate due to the enhancement of local fluid velocity adjacent to the disk. As the Ekman number decreases from ∞ to 4.42×10^{-5} the dimensionless interface temperature decreases by an average 3.7% under a low Reynolds number ($Re = 750$). The enhancement of Nusselt number due to rotation is primarily caused by enhancement of local fluid velocity adjacent to the rotating disk surface. The tangential velocity due to rotation combined with axial and radial velocities due to jet momentum results in an increased magnitude of velocity vector starting from the center of the disk. In the core region of the jet, rotation helps fluid particles to get spread out much faster as the particles change the direction of motion from axial to radial. Therefore, a large enhancement of local Nusselt number is obtained. It was found that at higher spinning rates or at larger radial locations, the boundary layer separates from the wall and causes an ineffective cooling. This type of behavior is

consistent with the results of Popiel and Boguslawski (1986) where in rotation dominated regime the impinging jet started being underscored by the fluid rejection of the rotating disk.

The effects of disk thickness variation on the solid–fluid dimensionless interface temperature and local Nusselt number are shown in Figs. 9 and 10, respectively. In these plots, silicon has been used as the disk material and water as the cooling fluid. The dimensionless solid–fluid interface temperature increases from the impingement region all the way to the end of the disk. It may be noted that the curves intersect with each other at a dimensionless radial distance of $r/r_d = 0.575$. Thicker disks generate more uniform dimensionless interface temperature due to a larger radial conduction within the disk. As the thickness of the solid disk increases, the Biot number increases. Therefore, the resistance to axial conduction across the disk increases. However, the values of Biot number are small indicating almost uniform temperature across the thickness of a silicon wafer. In addition, the dimensionless solid–fluid interface temperature and local Nusselt number distributions did not change much beyond a disk thickness of $b/d_n = 2$ indicating that the overall heat transport reached a convection–conduction equilibrium condition at the solid–fluid interface.

The local Nusselt number distributions for seven different nozzle-to-target spacing for water as the coolant at a spinning rate of 36.65 rad/s or 350 rpm and Reynolds number of 1250 are shown in Fig. 11. It may be noticed that the

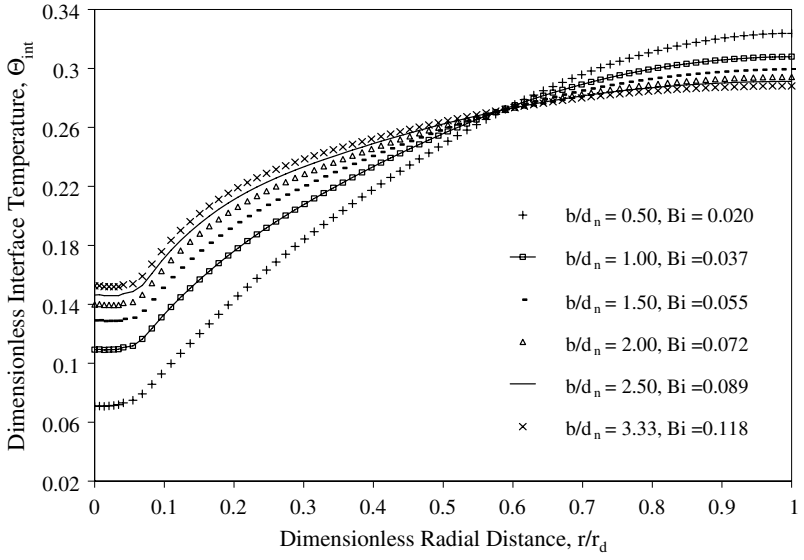

Fig. 9. Dimensionless interface temperature distributions for different silicon wafer thicknesses with water as the cooling fluid ($Re = 1000$, $Ek = 9.46 \times 10^{-5}$, $\beta = 2.67$).

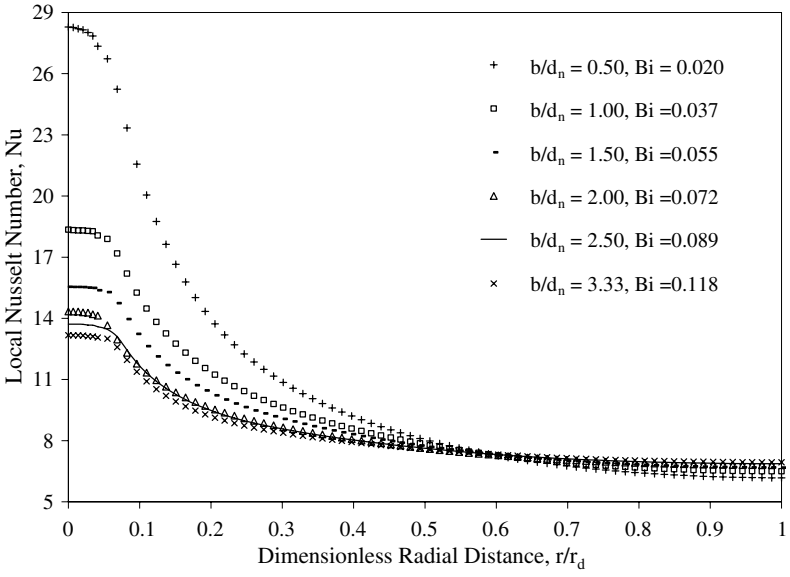

Fig. 10. Local Nusselt number distributions for different silicon wafer thicknesses with water as the cooling fluid ($Re = 1000$, $Ek = 9.46 \times 10^{-5}$, $\beta = 2.67$).

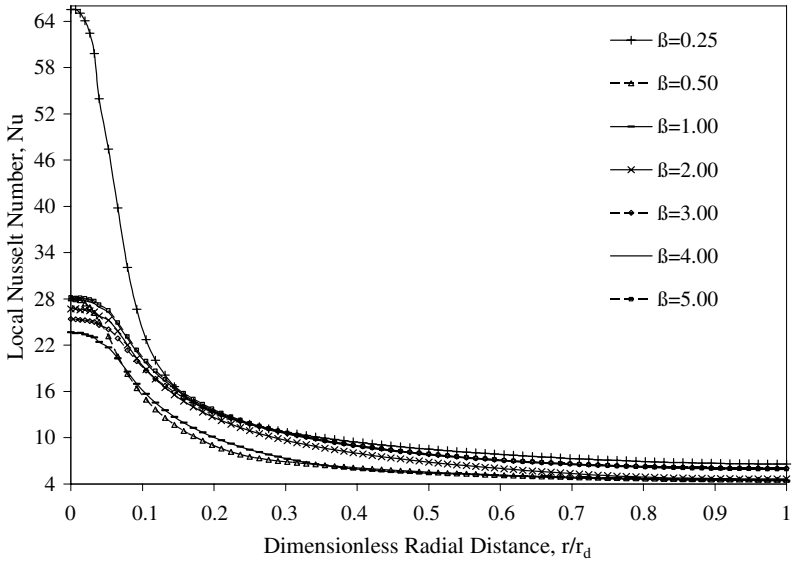

Fig. 11. Local Nusselt number distributions for a silicon disk with water as the cooling fluid for different nozzle to target spacing ($Re = 1250$, $Ek = 9.46 \times 10^{-5}$, $b/d_n = 0.5$).

impingement height quite significantly affects the Nusselt number distribution particularly at the stagnation region. It may be noticed that a very large Nusselt number is obtained when the nozzle is brought very close to the heated disk ($\beta = 0.25$). As the spacing is increased, the jet fluid needs to travel a larger distance through the existing fluid column between target and confinement disks and thereby looses its momentum. The minimum stagnation Nusselt number is seen for $\beta = 1$ and also the shape of the curve somewhat changes. There is also very small change in Nusselt number values at spacings greater than $\beta = 2$. This observation is in-line with the previous study by Hung and Lin (1994) for a confined jet impingement on a stationary disk.

Fig. 12 compares the dimensionless interface temperature results of the present working fluid (water) with three other coolants that have been considered in previous heat transfer studies, namely ammonia (NH_3), flouroinert (FC-77) and oil (MIL-7808) under a Reynolds number of 1500. Fig. 13 shows the corresponding local Nusselt number distributions. It may be noticed that water presents higher dimensionless interface temperature and lower local Nusselt number distribution in comparison with FC-77 and MIL-7808. MIL-7808 shows the largest variation of local Nusselt number primarily because of its larger variation of viscosity or Prandtl number with temperature. Ammonia provides a smaller Nusselt number compared to water because of its smaller Prandtl number.

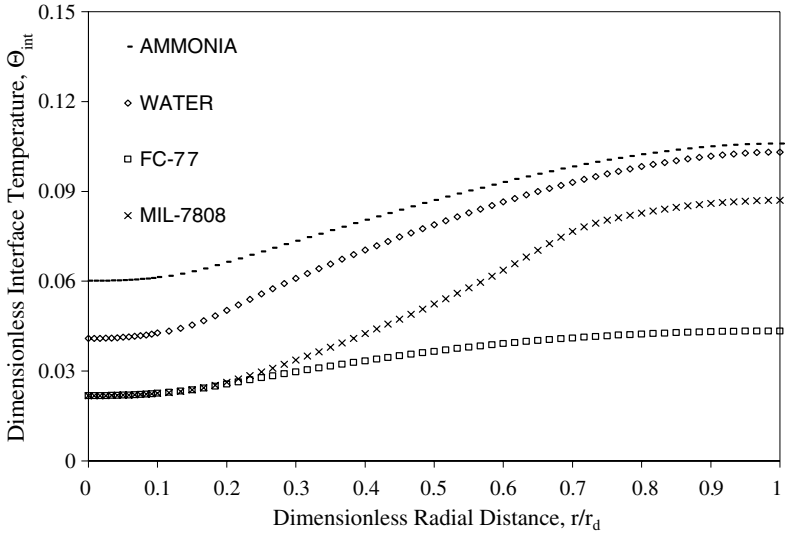

Fig. 12. Dimensionless interface temperature distributions for different cooling fluids for silicon as the disk material ($Re = 1500$, $Ek = 2.65 \times 10^{-4}$, $\beta = 2.67$, $b/d_n = 0.25$).

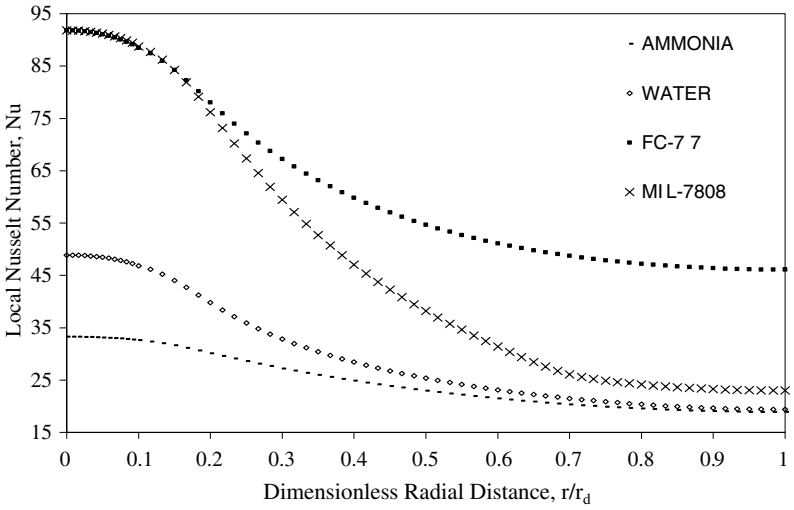

Fig. 13. Local Nusselt number distributions for different cooling fluids for silicon as the disk material ($Re = 1500$, $Ek = 2.65 \times 10^{-4}$, $\beta = 2.67$, $b/d_n = 0.25$).

Figs. 14 and 15 show the dimensionless solid–fluid interface temperature and local Nusselt number distribution plots respectively as a function of the dimensionless radial distance measured from the axisymmetric impingement axis for different solid materials with water as the working fluid. The numerical simulation was carried out for a set of materials, namely copper, aluminum, silver, Constantan, and silicon, having different thermophysical properties. Results for plain surface (zero thickness of the disk) are also plotted to identify the extent of conjugate effects. The temperature distribution plots reveal how the thermal conductivity of the solids affects the heat flux distribution that controls the local interface temperature. It may be noted that plain surface has the lowest temperature at the impingement axis and the highest at the outer edge of the disk. The interface temperature variation for Constantan is also quite large due to its lower thermal conductivity. As the thermal conductivity increases, the thermal resistance within the solid becomes lower and the interface temperature becomes more uniform as seen in the plots corresponding to copper and silicon. The cross-over of the curves of the five materials and plain surface occurred due to a constant fluid flow and heat flux rate that provides a constant thermal energy transfer for all circumstances. Narrow and elevated bell shape pattern is seen in Fig. 15 for all solid materials with lower thermal conductivity. Conversely high thermal conductivity materials like copper, aluminum and silver portrait a more uniform Nusselt number distribution in general. Biot number plays a fundamental role in conduction problems that involve surface convection effects. For all cases studied during the present analysis values for Biot number are small indicating that resistance to conduction

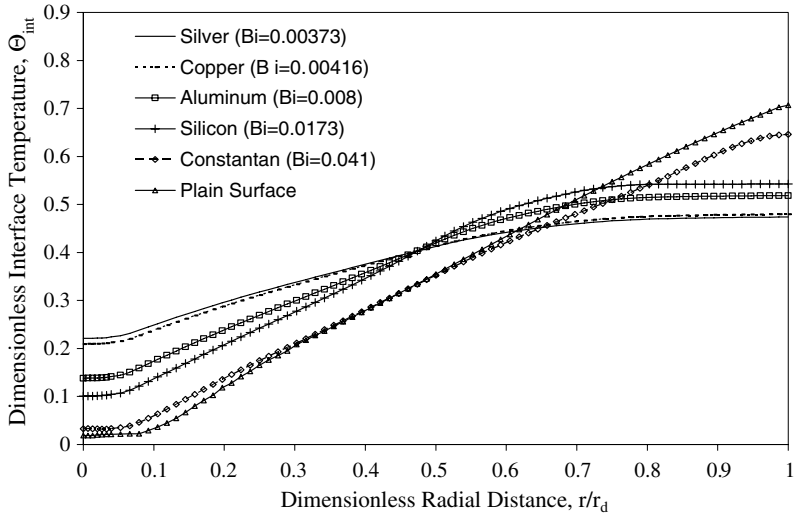

Fig. 14. Dimensionless interface temperature distributions for different solid materials with water as the cooling fluid ($Re = 900$, $Ek = 2.65 \times 10^{-4}$, $\beta = 2.67$, $b/d_n = 0.5$).

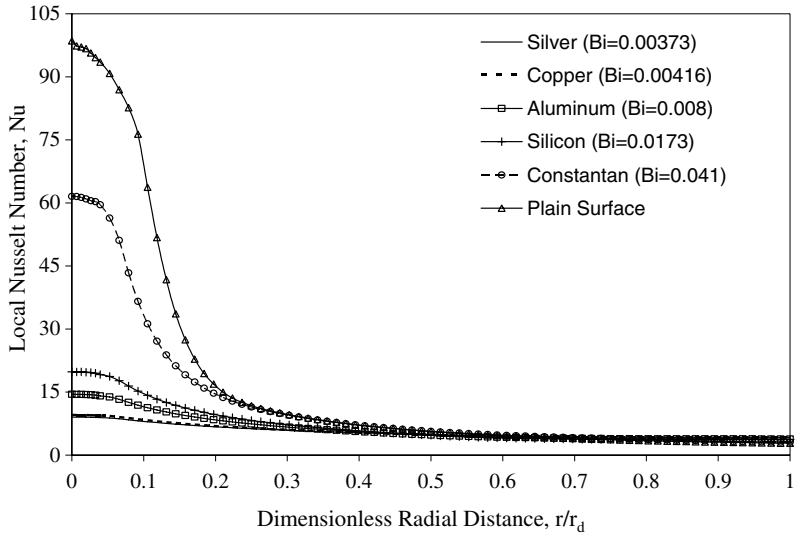

Fig. 15. Local Nusselt number distributions for different solid materials with water as the cooling fluid ($Re = 900$, $Ek = 2.65 \times 10^{-4}$, $\beta = 2.67$, $b/d_n = 0.5$).

within the solid is much less compared to the resistance to convection across the solid–fluid boundary.

Considering the trends of heat transfer enhancement as functions of thermal conductivity ratio, nozzle to target spacing, Prandtl number, Ekman number, and Reynolds number and by accommodating most of the transport characteristics of a confined liquid jet impingement cooling, a correlation was developed in the following form:

$$Nu_{av} = 1.97619 \cdot \beta^{0.0909} \cdot Re^{0.75} \cdot Ek^{-0.1111} \cdot \varepsilon^{-0.9} \quad (19)$$

In developing this correlation, all average Nusselt number data corresponding to the variation of different parameters were used. Only data points corresponding to water as the fluid were used because the number of average heat transfer data for other fluids were small. Fig. 16 gives the comparison between the numerical average Nusselt numbers to average Nusselt numbers predicted by Eq. (19). The average Nusselt number deviates in a range of −18.4% to +18.9% from the one predicted by Eq. (19). The mean deviation is 6.1%. The ranges of the dimensionless variables in this study are the following: $500 \leqslant Re \leqslant 1500$, $6.62 \times 10^{-5} \leqslant Ek \leqslant 2.65 \times 10^{-4}$, $0.5 \leqslant \beta \leqslant 5$, $Pr = 5.5$, $227.6 \leqslant \varepsilon \leqslant 697.5$. It should be noted from Fig. 16 that a large number of data points are very well correlated with Eq. (19). This correlation provides a convenient tool for the prediction of average heat transfer coefficient under confined liquid jet impingement on top of a spinning disk. The major difference between past studies and the present investigation is the accounting for conduction within the solid wafer and fluid for various materials, plus the nozzle to target spacing ratio as a part of the correlation.

One of the papers used for the validation of this numerical study was the experimental work carried out by Garimella and Rice (1995) using flouroinert (FC-77) as the coolant.

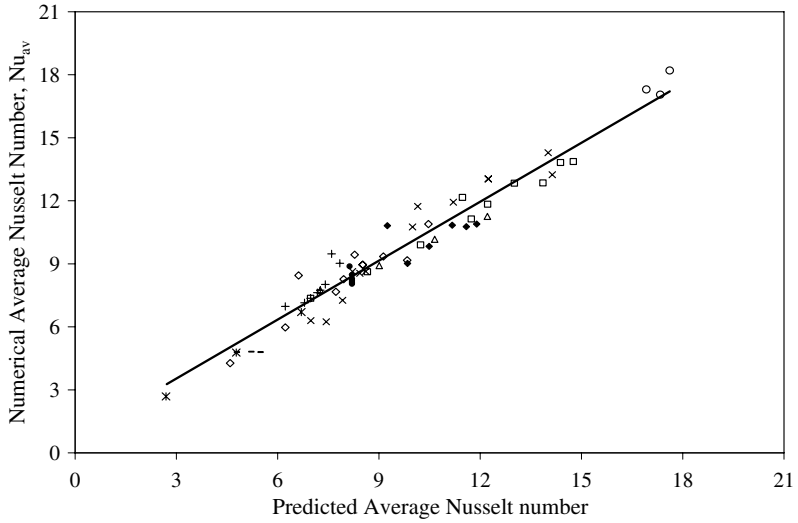

Fig. 16. Comparison of predicted average Nusselt number (Eq. (19)) with numerical data.

This liquid was tested for heat removal under confined liquid jet impingement on a stationary disk ($Ek = \infty$). The simulation attempted to duplicate the exact conditions of that experiment. Fig. 17 compares the variations of local Nusselt number distribution along the solid–fluid interface obtained from the simulation with the correlation developed from the experimental data. Considering the errors inherent in any experimental measurements (the reported uncertainty range of 0.13–3.2%) as well as discretization and round-off errors in the simulation, the comparison is quite satisfactory. A similar comparison was obtained with Ma et al. (1990).

The experimental work carried out by Carper et al. (1986) to determine the average heat transfer coefficient of a rotating disk, with an approximately uniform surface temperature, cooled by a single oil liquid jet impinging normal to the surface was also used for the validation of numerical results. The authors presented correlations that related the average Nusselt number to rotational Reynolds number, jet Reynolds number, and Prandtl number. The simulation has attempted to duplicate numerically the exact conditions of that experiment. The computation was conducted for three nominal values of T_J of 375, 331 and 320 K resulting in values of Pr of 87, 270 and 400, respectively. The rotational Reynolds number was kept constant at a value equal to 26,000. As a result of these behavior three distinct angular velocity values (Ω) had to be used: 14.66, 50.27 and 76.45 rad/s corresponding to the Prandtl numbers of 87, 270 and 400, respectively. The disk had a diameter of 10 cm and thickness of 2.54 cm and was made of 7075-T6 aluminum, a material with a relatively high thermal conductivity of 121.4 W/m K.

As seen in Fig. 18, the agreement of the results from the average Nusselt number correlation of Carper et al. (1986) with the present data is quite good. Three different plots

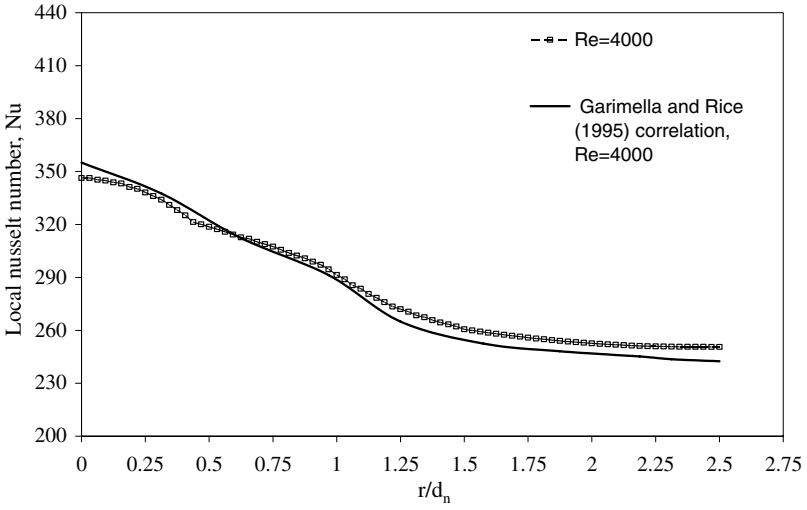

Fig. 17. Local Nusselt number distribution for a silver disk with FC-77 as the cooling fluid ($\beta = 4$, $Ek = \infty$, $q = 250$ kW/m^2).

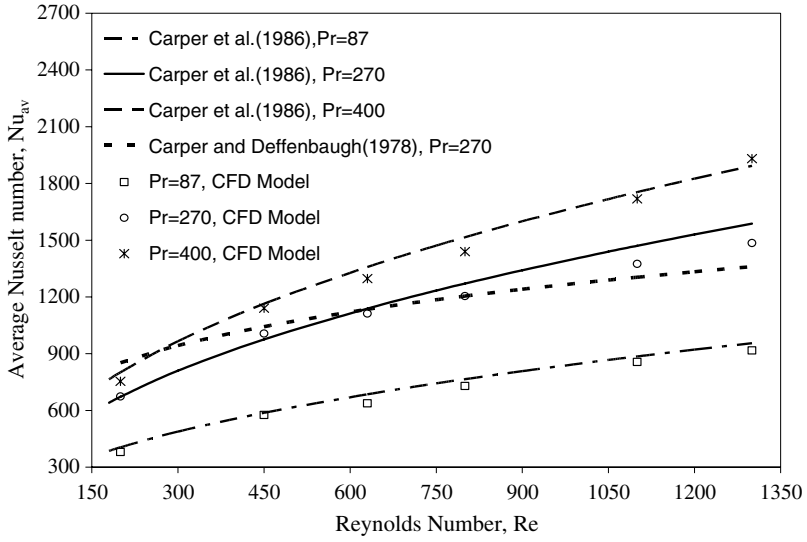

Fig. 18. Comparison of average Nusselt number with experimental data of Carper and Deffenbaugh (1978) and Carper et al. (1986) under various Reynolds numbers and three different Prandtl numbers of axisymmetric liquid oil jet impingement.

based on this correlation have been included in order to make a qualitative and quantitative comparison. The average Nusselt number uncertainties of Carper et al. (1986) range from 0.23% to 18.05% for all Prandtl numbers. An additional average Nusselt number plot was included from Carper and Deffenbaugh (1978) for Prandtl number of 270. The average Nusselt number uncertainties for Carper and Deffenbaugh (1978) correlation range from 1.96% to 20.2%. This validation with available experimental data may provide good level of confidence on the numbers obtained during present numerical simulation.

4. Conclusions

The solid–fluid dimensionless interface temperature, the local Nusselt number and local heat transfer coefficient shows a strong dependence on the following parameters: Reynolds number, rotational rate, impingement height, disk thickness, solid material properties, and fluid properties. Increasing the Reynolds number increases the local heat transfer coefficient distribution values over the entire solid–fluid interface. Simultaneously, this effect reduces the solid–fluid temperature and improves the cooling effectiveness of the process. In general, the rotational rate increases the local Nusselt number values over the entire solid–fluid interface except for a disk under high spinning rate where the thermal boundary layer separates from the wall and generates an ineffective cooling. Plate materials with higher thermal conductivity maintained a more uniform temperature distribution at the solid–fluid interface. Correlation for average Nusselt number under confined jet impingement cooling of a spinning disk is proposed in terms of Reynolds number, Ekman number, nozzle to target spacing ratio, and thermal conductivity ratio. The differences between numerical and predicted values are in the range from −18.4% to +18.9%. The mean value of the error is 6.1%. The numerical results compared reasonably well with available experimental measurements.

References

Bejan, A., 1995. Convection Heat Transfer. John Wiley and Sons, New York. Appendix C, pp. 595–602.

Brodersen, S., Metzger, D.E., Fernando, H.J.S., 1996a. Flows generated by the impingement of a jet on a rotating surface. Part 1: Basic flow patterns. Journal of Fluids Engineering 118, 61–67.

Brodersen, S., Metzger, D.E., Fernando, H.J.S., 1996b. Flows generated by the impingement of a jet on a rotating surface. Part 2: Detailed flow structure and analysis. Journal of Fluids Engineering 118, 68–73.

Burmeister, L.C., 1993. Convective Heat Transfer, second ed. John Wiley and Sons Inc., New York. Appendix C, pp. 581–590.

Carper Jr, H.J., Deffenbaugh, D.M., 1978. Heat transfer from a rotating disk with liquid jet impingement. In: Proceedings of the Sixth International Heat Transfer Conference, Toronto, Ontario, Canada, vol. 4. Hemisphere Public Corp., Washington, DC, pp. 113–118.

Carper, H.J. Jr., Saavedra, J.J., Suwanprateep, T., 1986. Liquid jet impingement cooling of a rotating disk. Transactions of the ASME 108, 540–546.

Chan, T.L., Leung, C.W., Jambunathan, K., Ashforth-Frost, S., Zhou, Y., Liu, M.H., 2002. Heat transfer characteristics of a slot jet impinging on a semi-circular convex surface. International Journal of Heat and Mass Transfer 45 (5), 993–1006.

Chang, C.T., Kocamustafaogullari, G., Landis, F., Downing, S., 1993. Single and multiple liquid jet-impingement heat transfer. Heat Transfer in Turbulent Flows, ASME HTD-246, 43–52.

El-Gabry, L.A., Kaminski, D.A., 2005. Experimental investigation of local heat transfer distribution on smooth and roughened surfaces under an array of angled impinging jets. Journal of Turbomachinery 127 (3), 532–544.

Faghri, A., Thomas, S., Rahman, M.M., 1993. Conjugate heat transfer from a heated disk to a thin liquid film formed by a controlled impinging jet. Journal of Heat Transfer 115, 116–123.

Fitzgerald, J.A., Garimella, S.V., 1997. Flow field effects on heat transfer in confined jet impingement. Journal of Heat Transfer 119, 630–632.

Fletcher, C.A.J., 1984. Computational Galerkin Methods. Springer Verlag, New York.

Garimella, S.V., Nenaydykh, B., 1996. Nozzle geometry effects in liquid jet impingement heat transfer. International Journal of Heat and Mass Transfer 39 (14), 2915–2923.

Garimella, S.V., Rice, R., 1995. Confined and submerged liquid jet heat transfer. Journal of Heat Transfer 117 (4), 871–877.

Hung, Y.H., Lin, Z.H., 1994. Effect of confinement plate on heat transfer characteristics of a circular jet impingement. ASME HTD-285, 101–109.

Hung, Y.H., Shieh, Y.R., 2001. Convective heat transfer from a rotating ceramic-based multichip disk with round jet impingement. In: Proceedings of the 2001 National Heat Transfer Conference, vol. 1, Anaheim, California, pp. 97–103.

Iacovides, H., Kounadis, D., Launder, B.E., Li, J., Xu, Z., 2005. Experimental study of the flow and thermal development of a row cooling jets impinging on a rotating concave surface. Journal of Turbomachinery 127 (1), 222–229.

Ichimiya, K., Yamada, Y., 2003. Three-dimensional heat transfer of a confined circular impinging jet with buoyancy effects. Journal of Heat Transfer 125 (2), 250–256.

Jiji, L.M., Dagan, Z., 1987. Experimental investigation of single phase multi-jet impingement cooling of an array of microelectronic heat sources. In: Proceedings of the International Symposium on Cooling Technology for Electronic Equipment, Pacific Institute for Thermal Engineering, HI, pp. 265–283.

Kang, H.S., Yoo, J.Y., 2002. Turbulence characteristics of the three-dimensional boundary layer on a rotating disk with jet impingement. Experiments in Fluids 33 (2), 270–280.

Li, C.Y., Garimella, S.V., 2001. Prandtl-number effects and generalized correlations for confined and submerged jet impingement. International Journal of Heat and Mass Transfer 44 (18), 3471–3480.

Ma, C.F., Sun, H., Auracher, H., Gomi, T., 1990. Local convective heat transfer from vertical heated surfaces to impinging circular jets. In: Proceedings of the Ninth International Heat Transfer Conference, vol. 2. Hemisphere, Washington, DC, pp. 441–446.

Ma, C.F., Li, D.Y., Guo, Z., 1997. Relationship between recovery factor and the viscous dissipation in a confined, impinging, circular jet of high Prandtl number liquid. International Journal of Heat and Fluid flow 18, 585–590.

Metzger, D.E., Bunker, R.S., Bosch, G., 1991. Transient liquid crystal measurements of local heat transfer on a rotating disk with jet impingement. Journal of Turbomachinery 113, 52–59.

Mochizuki, S., Inoue, T., 1990. Self-sustained flow oscillations and heat transfer in radial flow through co-rotating parallel disks. Experimental Thermal and Fluid Science 3, 242–248.

Nakoryakov, V.E., Pokusaev, B.G., Troyan, E.N., 1978. Impingement of an axisymmetric liquid jet on a barrier. International Journal of Heat and Mass Transfer 21, 1175–1184.

Özisik, M.N., 1993. Heat Conduction, second ed. John Wiley and Sons, New York. Appendix 1, pp. 657–660.

Polat, S., Huang, B., Mujumdar, A.S., Douglas, W.J.M., 1989. Numerical flow and heat transfer under impinging jets: A review. Annual Review Numerical Fluid Mechanics and Heat Transfer 2, 157–197.

Polat, S., Mujumdar, A.S., Douglas, W.J.M., 1991a. Impingement heat transfer under a confined slot jet. Part 1: Effect of surface thorough flow. Canadian Journal of Chemical Engineering 69, 266–273.

Polat, S., Mujumdar, A.S., Douglas, W.J.M., 1991b. Impingement heat transfer under a confined slot jet. Part 2: Effect of surface motion and thorough flow. Canadian Journal of Chemical Engineering 69, 274–280.

Popiel, C.O., Boguslawski, L., 1986. Local heat transfer from a rotating disk in an impinging round jet. Journal of Heat Transfer 108, 357–364.

Roy, S., Nasr, K., Patel, P., AbdulNour, B., 2002. Rectangular jet impingement heat transfer on a vehicle windshield. Journal of Thermophysics and Heat Transfer 16 (1), 154–157.

Saad, N.R., Douglas, J.M., Mujumdar, A.S., 1977. Prediction of heat transfer under an axisymmetric laminar impinging jet. Industrial and Engineering Chemistry Fundamental 16, 148–154.

Saniei, N., Yan, X., 2000. Experimental study of heat transfer from a disk rotating in an infinite environment including heat transfer enhancement by jet impingement cooling. Journal of Enhanced Heat Transfer 7 (4), 231–245.

Saniei, N., Yan, X., Schooley, W., 1998. Local heat transfer characteristics of a rotating disk under jet Impingement cooling. In: Proceedings of the 11th International Heat Transfer Conference, Kyongju, Korea.

Shevchuk, I.V., Saniei, N., Yan, X.T., 2003. Impingement heat transfer over a rotating disk: integral method. Journal of Thermophysics and Heat Transfer 17 (2), 291–293.

Shi, Y.L., Ray, M.B., Mujumdar, A.S., 2003. Effects of Prandtl number on impinging jet heat transfer under a semi-confined laminar slot jet. International Communications in Heat and Mass Transfer 30 (4), 455–464.

Silverman, I., Nagler, A., 2004. High heat flux cooling with water jet impingement. In: Proceedings of the ASME Heat Transfer/Fluids Engineering Summer Conference, vol. 1, Charlotte, North Carolina, pp. 277–288.

Thomas, S., Faghri, A., Hankey, W.L., 1991. Experimental analysis and flow visualization of a thin liquid film on a stationary and rotating disk. Journal of Fluids Engineering 113 (1), 73–80.

Tong, A.Y., 2003. A numerical study on the hydrodynamics and heat transfer of a circular liquid jet impinging onto a substrate. Numerical Heat Transfer, Part A 44, 1–19.

Vanyo, J.P., 1993. Rotating Fluids in Engineering and Science. Butterworth–Heineman, Massachusetts, pp. 233–264.

Webb, B.W., Ma, C.F., 1995. Single-phase liquid jet impingement heat transfer. Advances in Heat Transfer 26, 105–117.